EasyChair Preprint

№ 15331

Analysis of the Surface Acoustic Wave Modes Using Finite-Difference Time-Domain Method

Ziliang Pang

October 29, 2024

Analysis of the Surface Acoustic Wave Modes Using Finite-Difference Time-Domain Method

1st Ziliang Pang
School of Semiconductor and Physics,
North University of China
Shanxi, China
pzlliasdd@foxmail.com

***Abstract*—Surface acoustic waves are a widely utilized physical phenomenon. Their propagation can be described using partial differential equations with boundary conditions. Finite difference methods are particularly effective for solving these types of problems, and they have been extensively applied in research on surface wave propagation and scattering. This paper presents a time-domain finite difference analysis of surface acoustic wave propagation in zinc oxide piezoelectric materials. The analysis takes into account anisotropy, piezoelectric effects, and free boundary conditions. These insights are crucial for the design and optimization of surface acoustic wave devices based on zinc oxide materials.**

***Keywords*—Finite-difference time-domain (FDTD) methods, surface acoustic wave (SAW), zinc oxide(ZnO).**

I. Introduction

Discovered by Lord Rayleigh in 1885, the surface wave travels along the surface of a thick solid substrate, penetrating only to a depth of approximately one wavelength [1]. These waves cause atoms to oscillate in an elliptical path [2]. In anisotropic piezoelectric materials, the deformation of the lattice or strain waves leads to alterations in charge polarization, thereby producing electric fields. These electric fields further induce changes in strain as the wave moves, making a combination of mechanical and electric potential waves.

Today, the SAW technique is widely employed for signal filtering in televisions, mobile phones, radar systems. Every day, approximately 1 million SAW filters are produced and utilized daily in the signal communications industry. SAW devices have been shown to operate at frequencies ranging from tens of MHz to 10 GHz.These devices are known for their durability, reliability, and affordability, with no DC power consumption, which makes them widely used in both consumer and military electronics, especially in portable applications [3]. Apart from the filters, SAW is used in various other areas. SAW manage or transport electrons and holes, making them useful in quantum optics. In spintronics, SAW can extend the spin lifetime. Moreover, SAW could pave the way for advancements in quantum spintronics and quantum information processing. Additionally, SAW can control magnetization resonance in a ferromagnetic thin film. It is shown that SAW can interact with nanostructures, enabling the observation of intriguing quantum phenomena [4].

In this paper, the FDTD method is employed for the numerical analysis of surface acoustic wave propagation, successfully simulating these waves in anisotropic piezoelectric zinc oxide materials under stress-free boundary conditions. The simulation results indicate that increasing the amplitude of the input RF voltage can significantly enhance the amplitude of the surface acoustic waves in the zinc oxide material. The model developed in this paper is suitable for analyzing surface acoustic wave devices affected by surface skimming bulk wave (SSBW) interference and piezoelectric effects in zinc oxide. These numerical simulation techniques demonstrate substantial potential for device design and optimization, paving the way for high-quality surface acoustic wave zinc oxide devices.

II. Theory

A. Propagation of Surface Acoustic Waves

The acoustics displacements are obtained by the governing equation for acoustic waves in elastic solids, which is expressed as:

$$[\nabla_s]\,[c]\,[\nabla_s]^T\,\{u\} - \rho\frac{\partial^2}{\partial t^2}\{u\} + \{f\} = 0 \tag{1}$$

Where $[c]$ is materials properties, f is the mechanical loading condition, u is the acoustics displacements.

It is assumed that the surface wave propagates along the x-direction and the particle displacement fields as proportional to:

$$\{u\} \propto e^{-ikbz}e^{ik(vt-x)} \tag{2}$$

Where k is the wavenumber, v is the wave phase velocity and b is a constant.

Rayleigh waves are characterized by polarization components in the x and z directions. By removing the y direction components, we derive the following reduced governing equation for Rayleigh waves:

$$\left\{\begin{array}{c} u_x \\ u_y \\ u_z \end{array}\right\} = \left\{\begin{array}{c} u_{x1}^1\alpha_1 e^{-ikb_1 z} + u_{x1}^3\alpha_3 e^{-ikb_3 z} \\ 0 \\ u_{z1}^1\alpha_1 e^{-ikb_1 z} + u_{z1}^3\alpha_3 e^{-ikb_3 z} \end{array}\right\} e^{ik(vt-x)} \tag{3}$$

Where α_1 and α_3 are constants determined by v. By applying the zero-stress boundary conditions of

$$\sigma_{z|_{z=0}} = \tau_{xz|_{z=0}} = 0 \tag{4}$$

We can find the phase the velocity of waves in Eq(3).Figure1 shows a 2D illustration of the particle displacements induced by the Rayleigh waves. Figure 2 shows the vector diagram of the displacements caused by surface acoustic waves, along with the contour plot of their vector magnitudes.

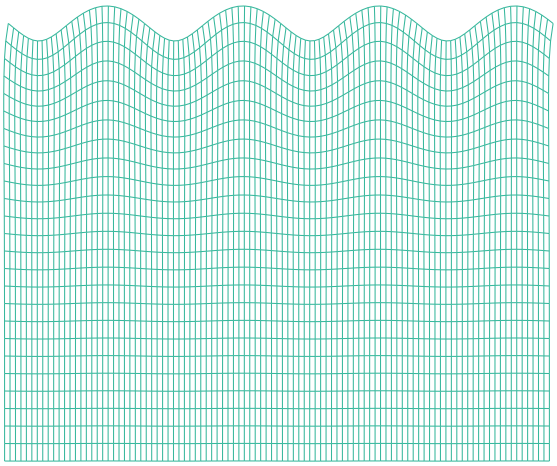

Fig. 1. Illustration of particle displacements generated by surface Rayleigh waves.

The deformed meshes are presented in a way that both the x and z displacements are in the right proportion to the displacement fields as a function of depth.

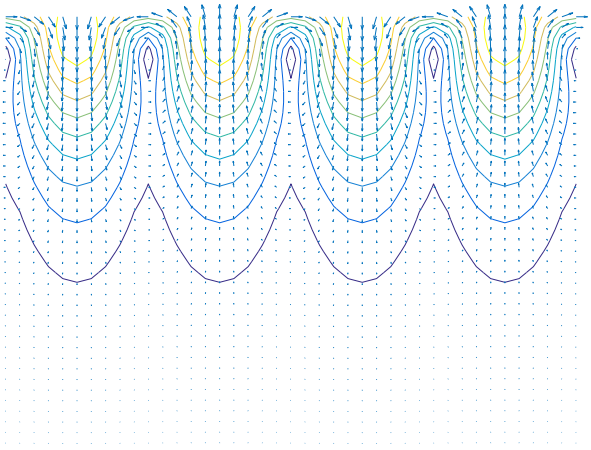

Fig. 2. Displacement vector diagram and contour map of vector magnitudes induced by surface acoustic wave.

B. Equations for Surface Acoustic Waves in Piezoelectric Solids

The coupling of mechanically and electrically induced stresses and electric displacements, resulting from direct and reverse piezoelectric effects, can be represented as:

$$\begin{aligned} \{T\} &= [c]\{S\} - [e]^T\{E\} \\ \{D\} &= [e]\{E\} + [e]\{S\} \end{aligned} \tag{5}$$

Where $[e]$ is the piezoelectric stress matrix, $[\epsilon]$ is the permittivity matrix, S is the strain vector, D is the electric displacement, E is the electric field vector.

By applying Gauss's law to the electric displacement and combining the piezoelectric coupling equations with (1), the equations for acoustic waves can be expressed as :

$$\begin{aligned} [\nabla_s]\left([c]\,[\nabla_s]^T\,\{u\} + [e]^T[\nabla]^T\{\phi\}\right) - \rho\frac{\partial^2}{\partial t^2}\{u\} = 0 \\ [\nabla]\left([e]\,[\nabla_s]^T\,\{u\} - [\epsilon][\nabla]^T\{\phi\}\right) = 0 \end{aligned} \tag{6}$$

Where ϕ is electrical potential. For the stiffness, piezoelectric stress constant and permittivity matrices of zinc oxide given below:

$$\begin{aligned} [c] &= 10^{10} \times \begin{bmatrix} 20.9 & 12.11 & 10.51 & 0 & 0 & 0 \\ 12.11 & 20.9 & 10.51 & 0 & 0 & 0 \\ 10.51 & 10.51 & 21.09 & 0 & 0 & 0 \\ 0 & 0 & 0 & 4.25 & 0 & 0 \\ 0 & 0 & 0 & 0 & 4.25 & 0 \\ 0 & 0 & 0 & 0 & 0 & 4.4 \end{bmatrix} (\mathrm{N/m^2}) \\ [e] &= \begin{bmatrix} 0 & 0 & 0 & 0 & -0.48 & 0 \\ 0 & 0 & 0 & -0.48 & 0 & 0 \\ -0.573 & -0.573 & 1.32 & 0 & 0 & 0 \end{bmatrix} (\mathrm{C/m^2}) \\ [\epsilon] &= 10^{-9} \begin{bmatrix} 0.085 & 0 & 0 \\ 0 & 0.085 & 0 \\ 0 & 0 & 0.102 \end{bmatrix} (\mathrm{F/m}) \end{aligned} \tag{7}$$

After substituting the parameters of the zinc oxide material into the equations(6) that does not contain the u_y, the following is obtained:

$$\begin{aligned} &\rho\frac{\partial^2 u_x}{\partial t^2} = 20.9\frac{\partial^2 u_x}{\partial x^2} + 14.76\frac{\partial^2 u_z}{\partial z \partial x} + 4.25\frac{\partial^2 u_x}{\partial z^2} - 0.573\frac{\partial^2 \phi}{\partial x^2} \\ &- 0.48\frac{\partial^2 \phi}{\partial z^2}, \\ &\rho\frac{\partial^2 u_z}{\partial t^2} = 21.09\frac{\partial^2 u_x}{\partial z^2} + 14.76\frac{\partial^2 u_x}{\partial x \partial z} + 4.25\frac{\partial^2 u_z}{\partial x^2} + 0.84\frac{\partial^2 \phi}{\partial x \partial z}, \\ &10^{-9}\left(0.085\frac{\partial^2 \phi}{\partial^2 x} + 0.102\frac{\partial^2 \phi}{\partial^2 z}\right) = -1.32\frac{\partial^2 u_z}{\partial z^2} + 1.053\frac{\partial^2 u_x}{\partial x \partial z} \\ &+ 0.48\frac{\partial^2 u_z}{\partial x^2} \end{aligned} \tag{8}$$

III. Computation Method

A. Finite Difference Method

In the field of surface acoustic wave numerical simulation, this paper utilizes one of the most powerful tools in computational electromagnetics, the Finite-Difference Time-Domain (FDTD) technique [5]. The main advantage of this technique is its ability to compute the propagation characteristics of waves in non-uniform and nonlinear media. At the same time, the FDTD method is based on the past field values at the nearest neighbor components, which provides high computational efficiency. Moreover, the time-marched arrays of field quantities generated by the FDTD method are well-suited for computer visualization, effectively illustrating the dynamics of the field [5].

After discretizing the wave equation using the central difference scheme, the displacement field values at time t can be expressed as:

$$
\begin{aligned}
u_{xi,k}^{n+1} =& -u_{xi,k}^{n-1} + 2u_{xi,k}^{n} + \left(\frac{20.9}{\rho}\right)\frac{\Delta t^2}{\Delta x^2}\left(u_{xi+1,k}^{n} + u_{xi-1,k}^{n}\right. \\
&\left. -2u_{xi,k}^{n}\right) + \left(\frac{14.76}{\rho}\right)\frac{\Delta t^2}{4\Delta x\Delta z}\left[\left(u_{zi+1,k+1}^{n} - u_{zi-1,k+1}^{n}\right)\right. \\
&\left. -\left(u_{zi+1,k-1}^{n} - u_{zi-1,k-1}^{n}\right)\right] \\
&+ \frac{4.25}{\rho}\frac{\Delta t^2}{\Delta z^2}\left(u_{xi,k+1}^{n} + u_{xi,k-1}^{n} - 2u_{xi,k}^{n}\right) \\
&+ \frac{-0.573}{\rho}\frac{\Delta t^2}{\Delta x^2}\left(\phi_{xi+1,k}^{n} + \phi_{xi-1,k}^{n} - 2\phi_{xi,k}^{n}\right) \\
&+ \left(\frac{-0.48}{\rho}\right)\frac{\Delta t^2}{\Delta z^2}\left(\phi_{zi+1,k}^{n} + \phi_{zi-1,k}^{n} - 2\phi_{zi,k}^{n}\right), \\
u_{zi,k}^{n+1} =& -u_{zi,k}^{n-1} + 2u_{zi,k}^{n} + \left(\frac{21.09}{\rho}\right)\frac{\Delta t^2}{\Delta z^2}\left(u_{zi,k+1}^{n} + u_{zi,k-1}^{n}\right. \\
&\left. -2u_{zi,k}^{n}\right) + \left(\frac{14.76}{\rho}\right)\frac{\Delta t^2}{4\Delta x\Delta z}\left[\left(u_{xi+1,k+1}^{n} - u_{xi-1,k+1}^{n}\right)\right. \\
&\left. -\left(u_{xi+1,k-1}^{n} - u_{xi-1,k-1}^{n}\right)\right] \\
&+ \frac{4.25}{\rho}\frac{\Delta t^2}{\Delta x^2}\left(u_{zi+1,k}^{n} + u_{zi-1,k}^{n} - 2u_{zi,k}^{n}\right) \\
&+ \frac{1.053}{\rho}\frac{\Delta t^2}{\Delta x^2}\left(\phi_{xi+1,k}^{n} + \phi_{xi-1,k}^{n} - 2\phi_{xi,k}^{n}\right) \\
&+ \left(\frac{0.48}{\rho}\right)\frac{\Delta t^2}{\Delta z^2}\left(\phi_{zi+1,k}^{n} + \phi_{zi-1,k}^{n} - 2\phi_{zi,k}^{n}\right).
\end{aligned}
\tag{9}
$$

In the above formula, the differences in displacement along the x and z directions are represented using subscripts separated by commas, where Δx and Δz denote the spatial steps in the x and z directions. To ensure the stability of the model, the discretized cell size is chosen to be 0.3 nm, and the time step is selected as 10 fs, which satisfies the stability conditions of the difference scheme.

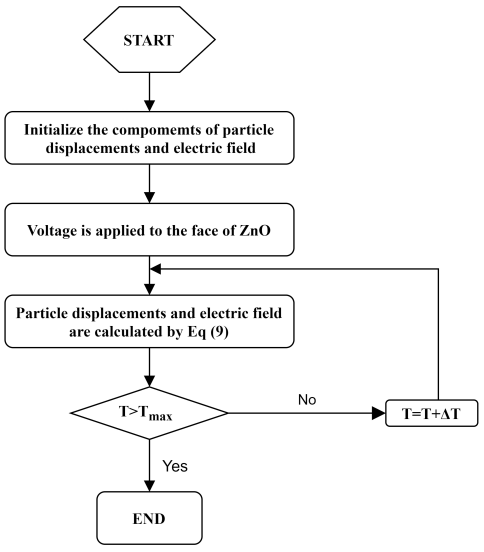

Fig. 3. FDTD methods for simulating surface acoustic waves.

The FDTD scheme used in this paper for surface acoustic wave propagation is summarized in Figure 3. Through the time iteration method, the next time step of the field component in Equation (9) is calculated using the past field values at the nearest neighbor components, ultimately generating the findings of the numerical analysis. Figure 4 presents a schematic diagram of the grid node calculations in the two-dimensional model.

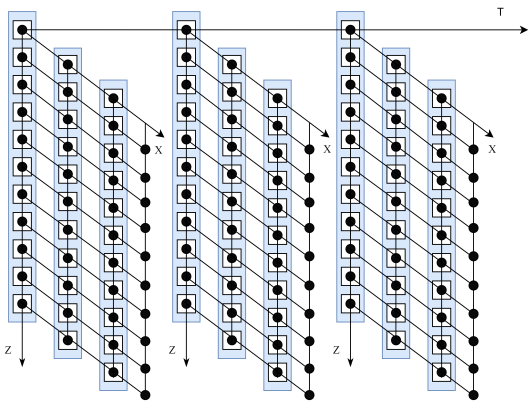

Fig. 4. Illustrative diagram of node calculations.

Compared to bulk waves, the numerical simulation of surface acoustic waves is more challenging and requires stricter boundary conditions for the free surface. The approach taken to address the free surface issue directly impacts the effectiveness of the numerical simulation of surface acoustic waves. This study employs a stress-free boundary condition for the boundary conditions at the air and zinc oxide interface. Levander proposed a method using mirror techniques to approximate the treatment of elastic free surfaces, which is now widely used as the Stress Image Method (SIM) [6].The stress mirror method is utilized to simulate the stress-free surface, where the stress-free surface is treated as a mirror, and a virtual layer is placed above the mirror to ensure that the axial stress is zero in both the upper and lower layers.

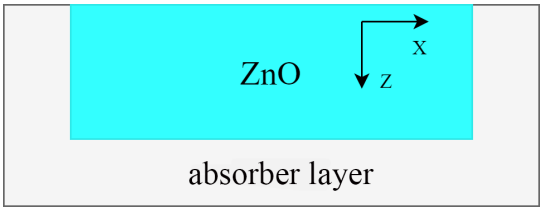

Fig. 5. Numerical configuration of the semi-infinite ZnO structure.

To simulate the wave equation, absorbing boundaries are required to account for the energy radiating outward. This study models the propagation of acoustic waves at the boundary using an absorbing layer with half-infinite boundary conditions on both sides and the bottom, as illustrated in Figure 5.

IV. Numerical Results

After the excitation source is applied, longitudinal surface skimming body waves (SSBWs), transverse SSBWs, and

surface acoustic waves propagate within the material. By comparing their propagation speeds, these acoustic waves can be easily distinguished. The longitudinal SSBW is the fastest among the three modes, while the propagation speed of the surface acoustic wave is slightly slower than that of the transverse SSBW. As shown in Figure 6 and Figure 7, the SSBW variation in components mainly occurs in the z direction, with minimal impact on the surface region. The primary modes include the longitudinal SSBW and the transverse SSBW. As the distance increases, the influence of the SSBWs on the surface region diminishes.

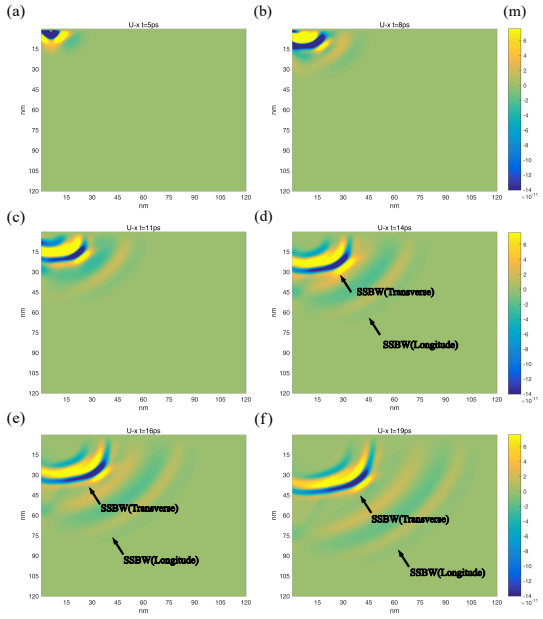

Fig. 6. FDTD methods for simulating surface acoustic waves.

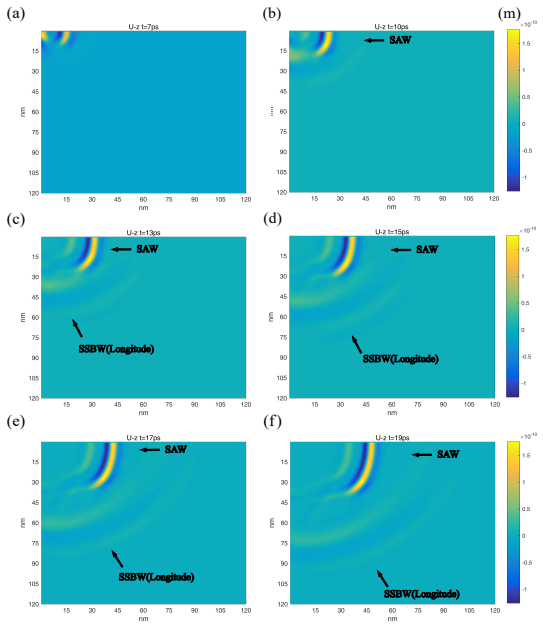

Fig. 7. FDTD methods for simulating surface acoustic waves.

Figure 6 and Figure 7 illustrate that over time, the acoustic wave components are largely confined to a region close to the surface, exhibiting a propagation mode characteristic of surface waves. It can be observed that the energy loss of the components propagating into the bulk of the piezoelectric material is significant. Additionally, SSBWs propagate just below the material's surface and are less sensitive to surface disturbances. As depicted in Figure 6 and Figure 7, the particle displacement caused by the surface wave is confined to a very narrow region near the surface. Since the energy of the surface acoustic wave is localized near the surface, surface devices become highly sensitive to disturbances and changes, allowing for the measurement of parameters such as temperature, humidity, pressure and mass.

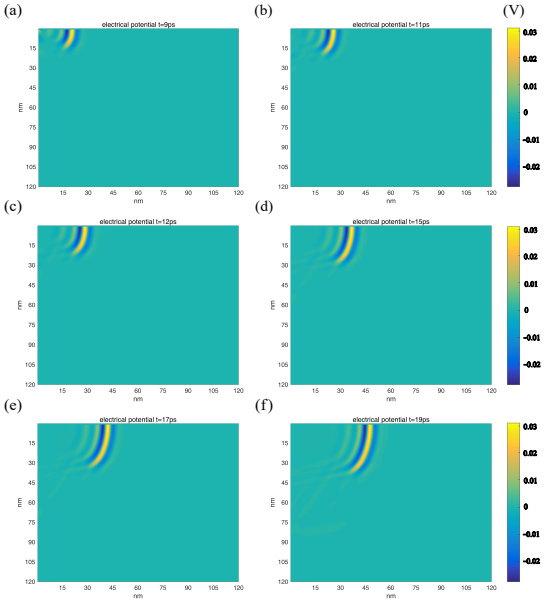

Fig. 8. FDTD methods for simulating surface acoustic waves.

Figure 8 shows the distribution of the electric potential generated by surface acoustic waves in the zinc oxide material during the time interval from 9 to 19 ps in both the horizontal and vertical directions. The propagation energy of the electric potential is primarily concentrated near the surface.

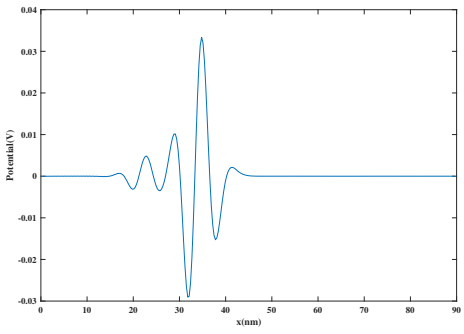

Fig. 9. FDTD methods for simulating surface acoustic waves.

Figure 9 illustrates the electric potential distribution curve on the surface of zinc oxide after applying a 1 V pulse radio frequency excitation at the position of x = 1 nm, at 15 ps. The electric potential change induced by the surface acoustic waves is vertical to the surface. The maximum amplitude of the potential waveform curve (the difference between the highest peak and the lowest valley) changes over time, as shown in Figure 10. As time progresses, the amplitude of the electric potential waveform traveling along the surface gradually decreases.

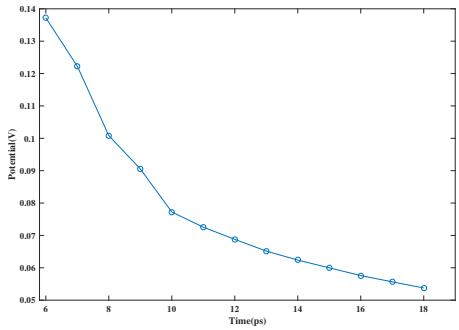

Fig. 10. FDTD methods for simulating surface acoustic waves.

V. Conclusion

This paper extended the FDTD scheme to analyze the propagation of surface acoustic waves in solid zinc oxide. The results indicate that this technique is suitable for analyzing surface acoustic devices with SSBW interference. Additionally, the method provides a reliable prediction of the electric potential propagation of surface acoustic waves in piezoelectric materials. In the future, these numerical simulation methods exhibit great potential for the design and optimization of surface acoustic piezoelectric devices.

References

[1] Rayleigh, Lord, D. Cl, and F. Rs, "On Waves Propagated along the Plane Surface of an Elastic Solid," *Proceedings of the London Mathematical Society*, 1885.

[2] Z. Guigen, *Bulk and Surface Acoustic Waves: Fundamentals, Devices, and Applications*. Jenny Stanford, 12 2021.

[3] Y. Lu, N. W. Emanetoglu, and Y. Chen, "Chapter 13 - ZnO Piezoelectric Devices," in *Zinc Oxide Bulk, Thin Films and Nanostructures*, C. Jagadish and S. Pearton, Eds., Oxford, 2006, pp. 443–489.

[4] H. Hou, "Low-dimensional electron transport and surface acoustic waves in gaas and zno heterostructures," Ph.D. dissertation, 2019.

[5] K.-Y. Wong and W.-Y. Tam, "Analysis of the frequency response of saw filters using finite-difference time-domain method," *IEEE Transactions on Microwave Theory and Techniques*, vol. 53, no. 11, pp. 3364–3370, 2005.

[6] A. Levander, "Fourth-order finite-difference p-s," *Geophysics*, vol. 53, pp. 1425–1436, 11 1988.